Effects of self-interaction correction on momentum density in copper

1999 J. Phys.: Condens. Matter 11 1683

(http://iopscience.iop.org/0953-8984/11/7/003)

J. Phys.: Condens. Matter **11** (1999) 1683–1695. Printed in the UK PII: S0953-8984(99)93165-X

Effects of self-interaction correction on momentum density in copper

Y Kubo†, Y Sakurai‡ and N Shiotani§

† Department of Physics, College of Humanities and Sciences, Nihon University, Setagaya, Tokyo 156, Japan
‡ The Institute of Physical and Chemical Research, Spring-8, Kamigouri, Akougun, Hyogo 678-12, Japan
§ Tokyo University of Fisheries, Kounan, Minato, Tokyo 108, Japan

Received 7 April 1998, in final form 4 December 1998

Abstract. The full-potential linearized APW (FLAPW) method is employed to find out effects of introducing the self-interaction correction (SIC) on the band structure, the Fermi surface geometry, electron wavefunctions and Compton profiles. Introduction of the SIC lowers and narrows the d bands. As the results, the theoretical Compton profiles are brought into a better agreement with the experimental profiles on one hand, and the area of the Fermi surface neck at the L point becomes too small to explain the dHvA result on the other hand.

1. Introduction

Electron momentum density $\rho(\boldsymbol{p})$ is a quantity of great importance because it relates directly to the electron wavefunctions and occupation in $\boldsymbol{k}$-space. It is experimentally obtainable via Compton scattering. Synchrotron radiation sources offer revolutionary new opportunities for exploiting Compton scattering as a tool in investigating electron momentum density in materials. Within an impulse approximation projections of the momentum density, given in equation (1) by $J(p_z)$, which is known as the Compton profile, can be deduced from the measured differential scattering cross-section [1],

$$J(p_z) = \iint \rho(\boldsymbol{p})\,\mathrm{d}p_x\,\mathrm{d}p_y \tag{1}$$

where the z-axis is along the x-ray scattering vector. In an independent particle model $\rho(\boldsymbol{p})$ is given as

$$\rho(\boldsymbol{p}) = (2\pi)^{-3}\sum_{\boldsymbol{k}_n,b}^{occ}\delta(\boldsymbol{k}+\boldsymbol{K}_n-\boldsymbol{p})\left|\int \psi_{\boldsymbol{k}_n,b}(\boldsymbol{r})\exp(-\mathrm{i}\boldsymbol{p}\cdot\boldsymbol{r})\,\mathrm{d}\boldsymbol{r}\right|^2 \tag{2}$$

$$\boldsymbol{k}_n = \boldsymbol{k}+\boldsymbol{K}_n \tag{3}$$

where $\psi_{\boldsymbol{k}_n,b}(\boldsymbol{r})$ is a wavefunction of an electron in the state $\boldsymbol{k}$ and band b, $\boldsymbol{K}_n$ are reciprocal lattice vectors and the sum runs over all the occupied states. The measurement of the Compton profile, therefore, gives information about both the occupation in $\boldsymbol{k}$-space and the electron wavefunctions.

Every band theoretical calculation of the electron momentum density has been based on the local density approximation (LDA) [2, 3]. It is well known, however, that when the LDA is applied to a tightly bound electron system, cancellation of self-Coulomb energy and self-exchange–correlation energy is not guaranteed and thus a spurious self-interaction is introduced

0953-8984/99/071683+13$19.50

[4]. The self-interaction correction (SIC) for the LDA in the density functional methods has been treated by several authors [4–9]. It has been found that the SIC plays an important role in determining the energy levels of electrons in a free atom [4]. This implies that the SIC is also important in calculating the energy bands of insulators and semiconductors because a considerable amount of charge is localized around the atomic site. In the case of crystals, compared to the case of free atoms, it is much more difficult to introduce the SIC into the self-consistent energy-band calculations. However, several ways of including the SIC for solids have been proposed to mainly discuss band gaps of semiconductors and insulators [5–8]. On the other hand, no established formula is known to take into account the SIC for the case of metals. Therefore, besides neglect of the quasi-particle nature of the electron system, the LDA based band theory has its own limitation to account for experimental Compton profiles when solids under investigation have filled narrow energy bands like the d bands in Cu. The treatment of this problem has been discussed by Perdew and Zunger [4]. Having examined the band structure of the metals near the end of the transition metal series, Norman [9] has found that the LDA with the SIC gives much better agreements with the experiments as to the relative positions of the d bands and the E–$\boldsymbol{k}$ dispersion relationship. However, so far the effects of introducing the SIC on the wavefunctions, the momentum densities and Compton profiles of metals have not yet been examined.

A comparison between the Compton profile obtained by the experiment and that calculated by band theory has been thought to display differences between the true quasi-particle nature of the electron system and the approximated one particle picture of it given by the LDA-based band theory. In this context, there have been many investigations on the Compton profiles of various solids [10–20] by both earlier low resolution and recent high resolution experiments and by various methods of band structure calculations with varying degrees of accuracy. It has been found in these studies that although the band theory reproduces characteristic features of the observed profiles very well, in particular the signatures of the Fermi surface, the theoretical profile is always higher than the experimental profile at low momenta, and the theoretical profile always bears sharper fine structures than the observed profile. The crystalline anisotropy of the observed Compton profiles has also been well accounted for by the geometry of the Fermi surface and the anisotropy in the momentum density given by the band theory. However, the scale of the anisotropy is always larger in the theory than in the experiment. The most recent study of Compton profiles of Cu has been carried out by Sakurai *et al* [23]. They have measured the profiles along the $\langle 100 \rangle$, $\langle 110 \rangle$ and $\langle 111 \rangle$ directions with a momentum resolution of 0.12 atomic units (au). In parallel with the measurements they have calculated the corresponding theoretical profiles in the Korringa–Kohn–Rostoker (KKR) scheme with a high degree of self-consistency and a great accuracy in evaluation of the momentum density. Their findings are the same as that summarized above.

The aim of the present study is reexamine to what extent the experimental profile obtained by Sakurai *et al* [23] can be explained by the LDA-based band theory without and with the SIC. For this purpose the full-potential linearized APW (FLAPW) method with and without the SIC is employed to solve the band structure problem and to calculate Compton profiles. In section 2 the theoretical calculations are described. In section 3 comparisons between the theory and the reported experiments on the geometry of the Fermi surface and Compton profiles are made and discussed. The summary and conclusions are given in the last section.

2. FLAPW calculations with and without the SIC

The FLAPW method is employed to examine the effects of introduction of the SIC to the exchange–correlation functional of von Barth and Hedin [24] on the band structure,

wavefunctions and Compton profiles. In the present calculation the SIC potential $V_\ell^{SIC}(r)$ is introduced for each angular momentum ℓ in a way similar to the SIC potential for atoms [8]. That is, $V_\ell^{SIC}(r) = 0$ in the interstitial region, and inside the inscribed sphere the $V_\ell^{SIC}(r)$ is calculated in the same way as in the free atom case except that a non-integer occupation number at each quantum state is allowed. Then, $V_\ell^{SIC}(r)$ is given as

$$V_\ell^{SIC}(r) = -W_\ell \left\{ \int \mathrm{d}\boldsymbol{r}' \rho_\ell(\boldsymbol{r}')|\boldsymbol{r} - \boldsymbol{r}'|^{-1} + V_{XC}^{LDA}(\rho_\ell(r)) \right\} \tag{4}$$

where V_{XC}^{LDA} is the exchange–correlation potential given by the LDA, $\rho_\ell(r)$ is the partial charge density and W_ℓ is the partial occupation number given by

$$W_\ell = \int_{\varepsilon_0}^{E_F} D^\ell(\varepsilon)\,\mathrm{d}\varepsilon. \tag{5}$$

Here, $D^\ell(\varepsilon)$ is the partial density of states with angular momentum ℓ, E_F is the Fermi energy and ε_0 is the lowest energy in the valence bands. The partial charge density ρ_ℓ is obtained from the solutions of the following radial Schrödinger equation with the spherical part $V^{LDA}(r)$ of the potential given by all the charge density and the SIC potential V_ℓ^{SIC} in the inscribed sphere:

$$\left[-(2r^2)^{-1} \frac{\mathrm{d}}{\mathrm{d}r} \left(r^2 \frac{\mathrm{d}}{\mathrm{d}r} \right) + \frac{\ell(\ell+1)}{2r^2} + V^{LDA}(r) + V_\ell^{SIC}(r) \right] \varphi_\ell(r) = E_\ell \varphi_\ell(r) \tag{6}$$

$$\rho_\ell(r) = (4\pi)^{-1} |\varphi_\ell(r)|^2 \tag{7}$$

$$E_\ell = \frac{1}{W_\ell} \int_{occ} \varepsilon D^\ell(\varepsilon)\,\mathrm{d}\varepsilon. \tag{8}$$

The above procedure is incorporated into the whole self-consistent scheme of the FLAPW calculations, and E_ℓ and W_ℓ are determined self-consistently. Figure 1 shows the final $V^{LDA}(r)$ and $V_\ell^{SIC}(r)$.

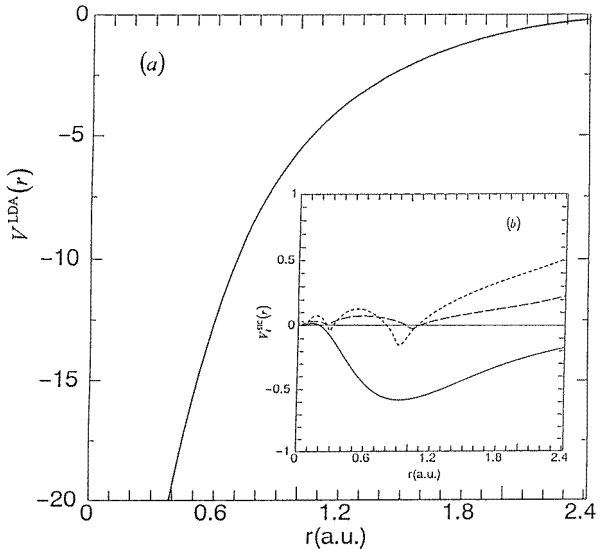

Figure 1. The potential in copper (Ryd). (*a*) The spherical part V^{LDA} of the potential determined by the FLAPW calculation without the SIC. (*b*) The partial component V_ℓ^{SIC} of the SIC potential for the angular momentum ℓ. The dotted, broken and full lines denote $\ell = 0$, $\ell = 1$ and $\ell = 2$, respectively

In both the FLAPW scheme and the FLAPW–SIC scheme, the energy values and the wavefunctions are calculated at 505 k-points in the irreducible (1/48)th of the Brillouin zone. The momentum density of the band electrons is calculated using 3143 reciprocal lattice vectors in equation (2). The number of band electrons in the calculated momentum density is more than 99.9% of the number of band electrons. The momentum density of the core electrons is also calculated in the FLAPW scheme and the FLAPW–SIC scheme. The SIC has no practical effect on the core profile because the core states are deeply situated. The resultant core profile is in very good agreement with that given by Biggs *et al* [25].

3. Results and discussion

From the SIC potential $V_\ell^{SIC}(r)$ shown in figure 1, the effects of the SIC on the band structure are predictable. $V_0^{SIC}(r)$ and $V_1^{SIC}(r)$ act as a small repulsive potential for the electrons with sp character, and $V_2^{SIC}(r)$ acts as an extra attractive potential for the electrons with d character. These lead to the following consequences. The width of the sp type band is little affected. The relative position of the d bands with respect to the Fermi energy is lowered by 2 eV, and the width of the d band is reduced by 15%. As the results the electrons in the d bands are more localized and the sp–d hybridization near the Fermi energy is much reduced. The geometry of the Fermi surface is summarized in table 1. The cross-sectional areas of the Fermi surfaces calculated by the FLAPW–SIC scheme are similar to those obtained by the FLAPW scheme, except the case of the area of the neck at the L point in which the comparison between the experiment and the FLAPW–SIC calculation shows a noticeable discrepancy. The reason of reduction of the neck size in the FLAPW–SIC calculation is explained as follows: the SIC lowers the d bands with respect to the Fermi energy, as a consequence the sp–d hybridization in the sixth band is reduced, and this leads to lifting of the L_2' state towards the Fermi energy and thus reducing the occupied volume around the L point.

Table 1. The de Haas–van Alphen frequencies of some symmetry orbits in units of frequency $\times 10^8$ G. LDA and SIC denote the results calculated by the FLAPW scheme without and with the SIC, respectively. EXP denotes the experimental values [30].

Orbit	Direction	LDA	SIC	EXP
Neck	⟨111⟩	0.296	0.090	0.218
Belly	⟨100⟩	6.463	6.343	5.998
Belly	⟨111⟩	6.167	6.300	5.814
Dog's bone	⟨110⟩	2.427	2.637	2.514
Rosette	⟨100⟩	2.427	2.491	2.462

The radial wavefunctions at two representative energies are shown in figure 2. The states near the bottom of the d bands are more affected by the introduction of the SIC than those near the top of the d bands. The corresponding radial momentum wavefunctions are shown in figure 3. It is found that the introduction of the SIC pushes the momentum wavefunction out toward higher momenta. It is noted that this effect of the SIC is particularly noticeable for the states near the bottom of the d bands. The effect of the SIC on momentum density $\rho(\boldsymbol{p})$ of equation (2) is shown in figure 4 where $\boldsymbol{p}$ is taken on the three symmetry axes. Introduction of the SIC reduces the momentum density in the region between 0 and 2.5 au, and increases it beyond 2.5 au. To avoid misunderstanding, it should be mentioned that when $\boldsymbol{p}$ is on an axis of general direction, reduction of the momentum density in small momenta and increase of it in high momenta is true, but the crossing is not necessarily around 2.5 au. When $\rho(\boldsymbol{p})$ is doubly integrated according to equation (1) to make the Compton profile, the reduction of

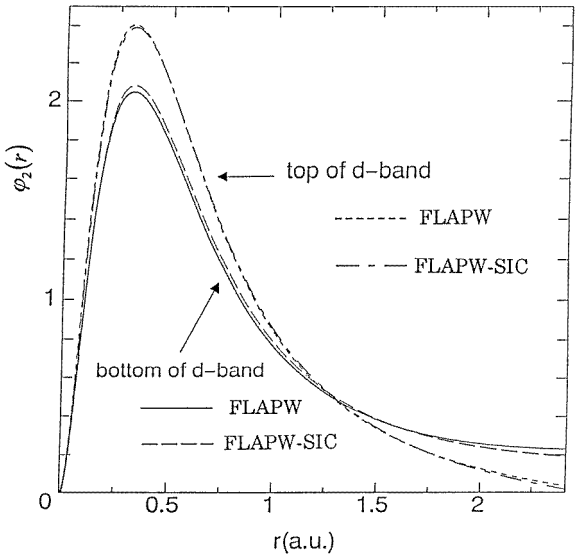

Figure 2. Radial wavefunctions $\varphi_2(r)$ of the d electrons at the energies of the bottom and the top of the d bands. FLAPW (full and broken lines) and FLAPW–SIC (dashed and chain lines) denote the results calculated by the FLAPW scheme without and with the SIC, respectively. They are normalized to unity within the inscribed sphere.

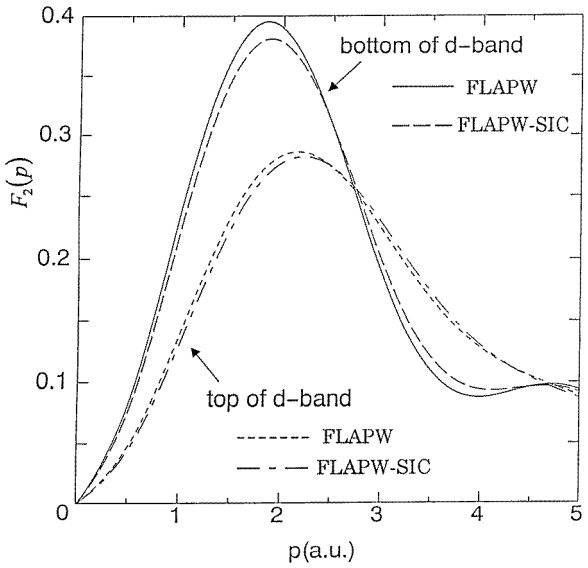

Figure 3. Radial momentum wavefunctions $F_2(p)$ which correspond to the radial wavefunctions shown in figure 2.

momentum density in small momenta and the increase of it in large momenta is retained but the crossing point seen in figure 4 for only three symmetry axes is not retained. The integrated results are shown in figure 5 together with the experimental profiles. The overall shapes of the profiles calculated with the SIC are always lower in small momenta (0–1 au) and higher in

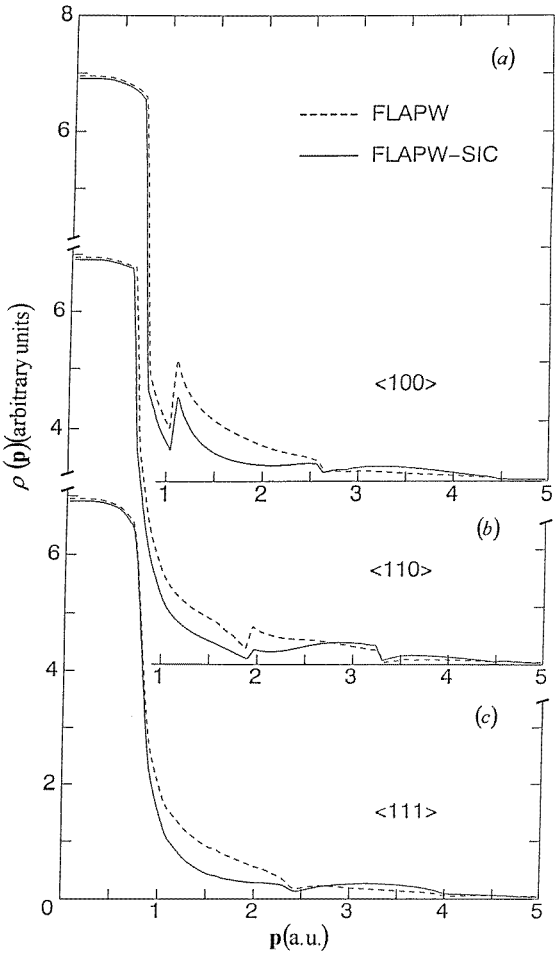

Figure 4. Theoretical three-dimensional momentum densities $\rho(\boldsymbol{p})$ on (*a*) ⟨100⟩, (*b*) ⟨110⟩ and (*c*) ⟨111⟩ axes calculated by the FLAPW (broken lines) and FLAPW–SIC (full lines) schemes.

the middle momenta (1–4 au) than those calculated without the SIC. Beyond 4 au, although they are indistinguishable in the figure, the profiles calculated with the SIC are always slightly higher than those calculated without the SIC. Compared with the experimental profiles, the theoretical profiles calculated without the SIC are higher in small momenta and lower in large momenta than the observed profiles. This fact is consistent with the most recent study on Cu by Sakurai *et al* [23]. The trend has been consistently seen in previous studies on other solids as well. Introduction of the SIC reduces the discrepancy between theory and experiment to a large extent, but not completely. The effect of introduction of the SIC is also clearly seen in the anisotropy of the profiles. The anisotropy is reduced in the FLAPW–SIC scheme as shown in figure 6. This is because the anisotropy caused by the d bands is reduced by the localization of the electrons in the d bands.

Figure 7 is for examination of the differences between the theoretical profiles and the observed ones. Referring to the difference between the FLAPW profiles and the experimental profiles, the origin of the significant discrepancy around $p_z = 0$ has been discussed by Lam

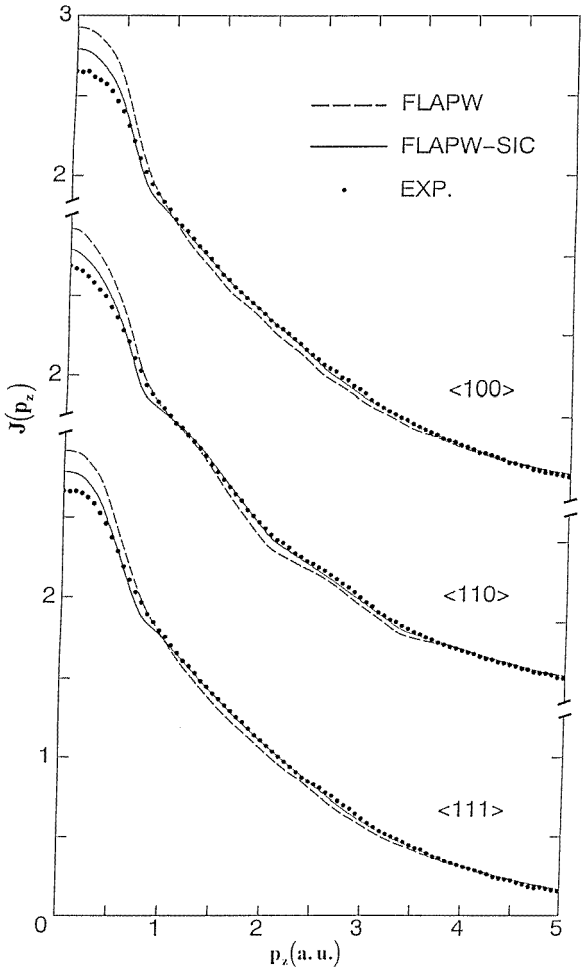

Figure 5. Valence electron Compton profiles along the ⟨100⟩, ⟨110⟩ and ⟨111⟩ directions. The theoretical profiles calculated by the FLAPW schemes without (broken lines) and with (full lines) the SIC are convoluted with the experimental resolution. The experimental profiles (EXP.) are taken from [23].

and Platzman [26], Bauer [27], and Bauer and Schneider [22, 28]. When the LDA is applied to the formal expression of momentum density, an exchange–correlation correction has to be added to the expression of one particle momentum density. This is the so-called Lam–Platzman correction. Although the Lam–Platzman correction helps to reduce the discrepancy to a certain extent as shown by Bauer and Schneider [28], the evaluation of the correction is not done without uncertainties because the electrons in the d bands cannot be treated as a homogeneous electron gas. For this reason the calculation of the Lam–Platzman correction term is not carried out in the present work. The difference curve along the [110] direction has local minima at around 2.0 au and 3.3 au, and local maxima at around 1.2 au and 2.7 au. As pointed out by Bauer and Schneider [22, 28], the local maxima appear every p_z where the integration plane of equation (1) contains the net of the reciprocal lattice points. This particular feature led Bauer and Schneider to discuss the effects of electron correlation in terms of non-zero and

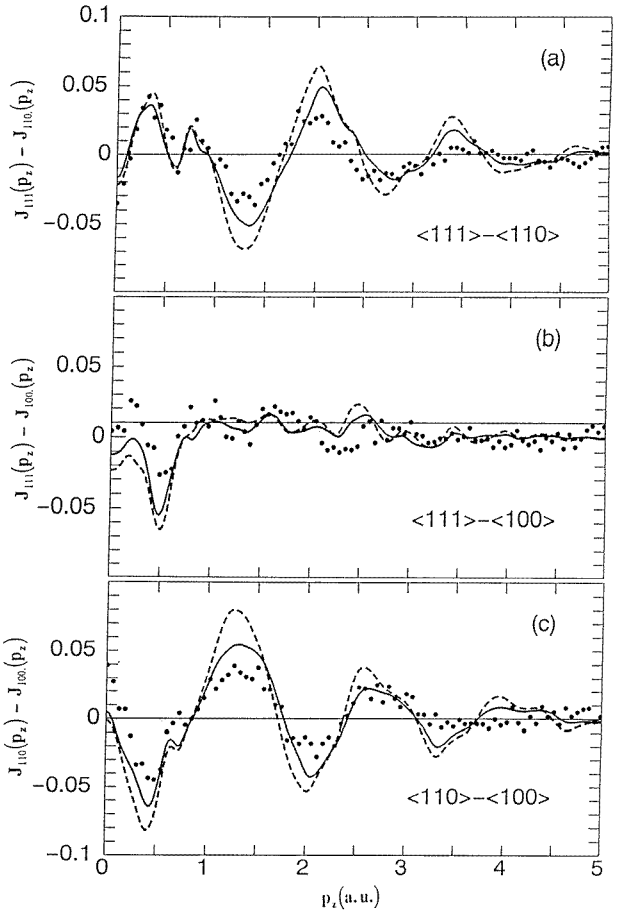

Figure 6. Experimental (dots [23]) and theoretical (broken line, FLAPW; full line, FLAPW–SIC) crystalline anisotropies of the Compton profiles. (a) ⟨111—110⟩, (b) ⟨111–100⟩ and (c) ⟨110–100⟩.

non-unity occupation number in $\boldsymbol{k}$-space. If the reason for the appearance of the local maxima is passing of the integration plane through the net of the reciprocal lattice points, from simple geometrical consideration, the local maxima should appear around 0.9 au and 1.8 au in the difference curve along the [100] direction. However, no such local maxima are found in the present study. It is obvious that the origin of the local extremes in the [110] difference curve is that the theoretical profile has more salient inflection at around 1.2 au, 2.0 au, 2.7 au and 3.3 au than the experimental profile. Detailed band-wise analyses shown in figure 8 reveal that these inflections are the resultants of all the contributions from the occupied states. Referring to the difference between the FLAPW–SIC profiles and the experimental profiles, the difference at $p_z = 0$ is drastically reduced, but a new large difference peak appears at around 0.75 au in every direction. The above mentioned local maxima and minima in the [110] curve nearly disappear. The origin of the peak at around 0.75 au may be seen in figures 5 and 8. In figure 5 the FLAPW–SIC profile has a stronger inflection at 0.75 au in every direction than the FLAPW profile. The crossing of the FLAPW–SIC profile and the experimental profile occurs at smaller p_z than that of the FLAPW and the experimental profile. Where the crossing occurs depends on the overall shape of the profile, therefore the position itself of crossing has little meaning.

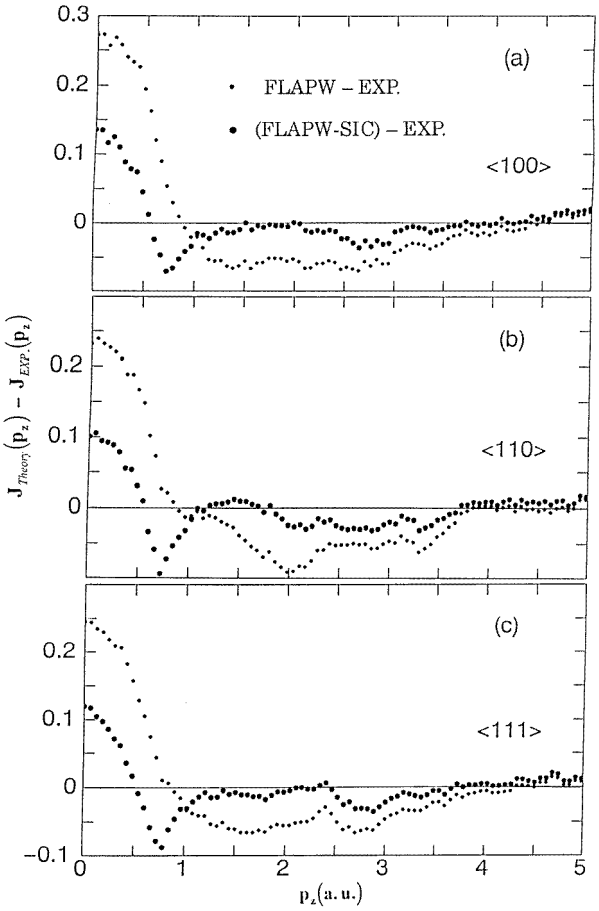

Figure 7. Difference between theory and experiment. The small dots represent the theoretical profile calculated without the SIC minus the experimental profile [23]. The large dots represent the theoretical profile calculated with the SIC minus the experimental profile.

The inflection at around 0.75 au is traced back to the effect of the SIC. In figure 8 it is seen that the salient difference between the FLAPW and the FLAPW–SIC is in the first and sixth band contributions. The first band contribution of the FLAPW–SIC is smaller than that of the FLAPW in the range of 0–0.75 au, and larger beyond this region. The FLAPW–SIC profile has a stronger inflection around 0.75 au than the FLAPW profile. The lowering of the d bands due to the SIC compresses the first band, and, as a result, produces more higher momentum components in momentum density. On the other hand, the sixth band contributions in the FLAPW–SIC is the other way around because of the reduction of the sp–d hybridization. The strong inflection at around 0.75 au is mostly the resultants of these two contributions. This is common in the other two directions. The local minima at around 2.0 and 3.3 au in the [110] difference curve of the FLAPW profile and the experimental one almost disappear when the SIC is introduced. The reason for this is also explained mostly by the contributions from the first and sixth bands. In figure 8 for both the FLAPW and the FLAPW–SIC profiles the first band contribution peaks at around 2.0 and 3.0 au, while the the sixth band contribution dips at around 2.0 and 3.3 au. The first band contribution of the FLAPW is smaller than that

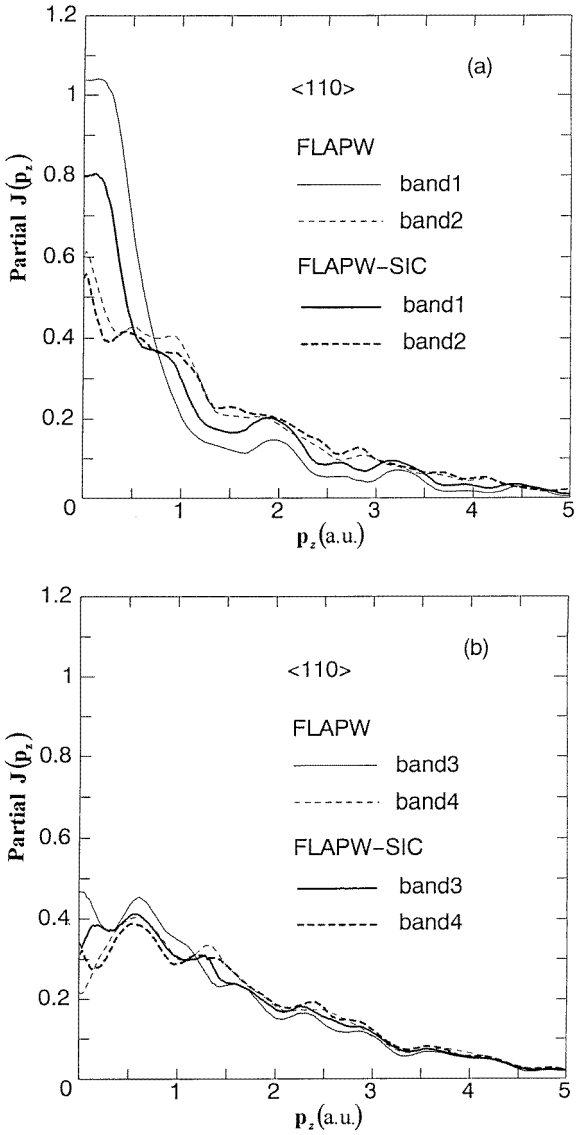

Figure 8. Band-wise analyses of the theoretical Compton profiles along the ⟨110⟩ direction calculated by the FLAPW and FLAPW–SIC schemes.

of the FLAPW–SIC, while the sixth band contribution of the FLAPW is larger than that of the FLAPW–SIC. Therefore, adding the first and the sixth band contributions leaves stronger minima in the FLAPW profile at around 2.0 and 3.3 au than those in the FLAPW–SIC.

In order to illustrate this situation more clearly the character-wise analyses of the number of charges in each band are performed and the results are listed in table 2. Referring to figure 8 and table 2, we can see that introduction of the SIC reduces the s and p components and increases the d component of the charge density of the first band. This change in the partial charge density is reflected in the first band partial profile in the way that it decreases significantly in low momenta and increases in high momenta. In the second and third bands a decrease of the

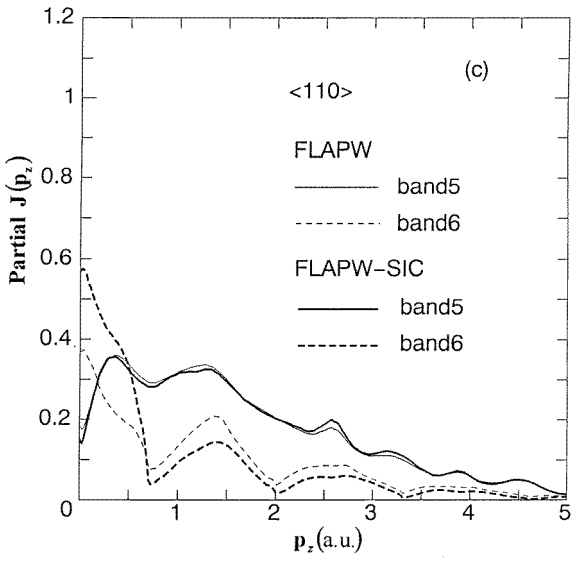

Figure 8. (Continued)

Table 2. The character-wise and band-wise analyses of the charge density. Band 1 means the first band. Out denotes the charge density in the interstitial region.

		Band 1	Band 2	Band 3	Band 4	Band 5	Band 6	Total
s	LDA	0.4480	0.0066	0.0216	0.0046	0.0046	0.0480	0.5334
	SIC	*0.2452*	*0.0264*	*0.0274*	*0.0148*	*0.0088*	*0.1790*	*0.5016*
p	LDA	0.1712	0.0838	0.0974	0.0376	0.0084	0.0900	0.4884
	SIC	*0.0516*	*0.0448*	*0.0546*	*0.0314*	*0.0068*	*0.1800*	*0.3692*
d	LDA	1.0628	1.7892	1.7904	1.9110	1.9698	0.8120	9.3352
	SIC	*1.5116*	*1.8248*	*1.8466*	*1.9082*	*1.9666*	*0.5018*	*9.5596*
Out	LDA	0.3180	0.1202	0.0906	0.0468	0.0170	0.0500	0.6426
	SIC	*0.1916*	*0.1040*	*0.0712*	*0.0456*	*0.0178*	*0.1390*	*0.5692*

p components and an increase of the d components are found, which leads to a similar change in the partial profiles of these bands as that in the first band profile. In the fourth and fifth bands there is not much change in the partial charge density nor in the partial profiles of these bands. In the sixth band a significant increase of the s and p components and a large decrease of the d component are observed, which is reflected in the change of the partial profile in the way that it increases significantly in low momenta and decreases in high momenta. In short, upon introduction of the SIC the occupied states in the lower five bands become significantly d-like while those in the sixth band become more sp-like. As the results, the charge distribution becomes less anisotropic. As for the anisotropies, the theoretical calculations with the SIC and without the SIC explain very well the oscillatory behaviour of the observed anisotropies. However, the scale of the calculated anisotropy by the LDA is larger than that of the observed anisotropy. Introduction of the SIC reduces the anisotropy of the momentum density because of the above mentioned effect. However, it does not bring the theory in complete agreement with the experiment.

4. Summary and conclusion

The Compton profiles of Cu along the ⟨100⟩, ⟨110⟩ and ⟨111⟩ directions have been computed in the FLAPW scheme, and in the FLAPW scheme with the self-interaction correction (FLAPW–SIC). Introduction of the SIC lowers the position of the d bands with respect to the Fermi energy, and narrows the width of the d bands, and also increases the number of d-like electrons. As the results, regarding the Fermi surface geometry, the area of the neck is reduced so much that it does not agree with the dHvA result. On the other hand, introduction of the SIC extends the momentum density of the electrons in the d bands further in higher momenta, which leads to reduction of the discrepancy between theory and experiment in the overall shapes of the profiles and of the scale of the crystalline anisotropies to a certain extent.

The reduction of the neck radius and the appearance of the new peak around $\boldsymbol{p}_z = 0.75$ au in the difference between theory and experiment (figure 7) due to introduction of the SIC are thought to be related to the treatment of the SIC in the atomic model. That is, in the present treatment angular momentum state is treated independently as far as the SIC potential is concerned; therefore the modification in the $\ell = 2$ states due to the SIC potential is not reflected in determining the states of $\ell = 0$ and 1. This leads to that lowering of the d bands, which reduces the sp–d hybridization, and makes the sixth band contribution more sp electron like as shown in figure 8(c) and table 2. If one aims at the complete self-consistent treatment of the SIC, one may have to solve the following coupled equations [4]

$$[H_{LDA} + V_s^{SIC}(\boldsymbol{r})]\varphi_s(\boldsymbol{r}) = \sum_{s'} E_{s,s'}\varphi_{s'}(\boldsymbol{r}) \tag{9}$$

$$V_s^{SIC}(\boldsymbol{r}) = 2\int \frac{|\varphi_s(r')|^2}{|\boldsymbol{r} - \boldsymbol{r}'|}\,\mathrm{d}\boldsymbol{r}' + V_{XC}^{LDA}(|\varphi_s(\boldsymbol{r})|^2, 0) \tag{10}$$

where H_{LDA} represents the LDA Hamiltonian, φ_s is a general one-electron state and V_{XC}^{LDA} is the LDA exchange–correlation potential. The Lagrange multipliers $E_{s,s'}$ ensure the orthogonality of $\varphi_s(\boldsymbol{r})$ which is violated by the present state dependence of the SIC potential.

The present theoretical studies indicate that when one deals with properties which are mostly determined by the states near the Fermi energy such as the Fermi surface geometry the usual LDA scheme works well, but for the properties which involve all the states from the bottom of the bands to the Fermi energy the usual LDA scheme does not work well. In both cases the position of the filled d bands is essential. Although the SIC potential employed in this study is not a uniquely determined one nor rigorously formulated, the present results suggest that some kind of correction to the LDA potential is need to explain the experimental results consistently. The origin of the remaining discrepancy in the shape of the Compton profile between theory and experiment may now be ascribed to the quasi-particle nature of the electron system, in particular to the non-unity and non-zero occupation in $\boldsymbol{k}$-space. Evaluation of the occupation number from the spectral functions as was done by Kubo [12] for Li and Na with use of the GW approximation [29] is the most meaningful and practical way to go beyond the LDA.

Acknowledgment

The present work was carried out under proposals No 92-G257, and No 94-G351 of the Photon Factory.

References

[1] See, e.g. Cooper M J 1985 *Rep. Prog. Phys.* **48** 415
[2] Hohenberg P and Kohn W 1964 *Phys. Rev.* B **136** 864
[3] Kohn W and Sham L J 1965 *Phys. Rev.* **140** A1133
[4] Perdew J P and Zunger A 1981 *Phys. Rev.* B **23** 5048
[5] Heaton R A, Harrison J G and Lin C C 1983 *Phys. Rev.* B **28** 5992
[6] Hatsugai Y and Fujiwara T 1986 *Phys. Rev.* B **34** 9042
[7] Ishii Y and Terakura K 1990 *Phys. Rev.* B **42** 10 924
[8] Hamada N and Ohnishi S 1986 *Phys. Rev.* B **34** 9042
[9] Norman M R 1984 *Phys. Rev.* B **29** 2956
[10] Sakurai Y, Tanaka Y, Bansil A, Kaprzyk S, Stewart A T, Nagashima Y, Hyodo T, Nanao S, Kawata H and Shiotani N 1995 *Phys. Rev. Lett.* **74** 2252
[11] Schülke W, Stutz G, Wohlert F and Kaprolat A 1996 *Phys. Rev.* B **54** 14 381
[12] Kubo Y 1997 *J. Phys. Soc. Japan* **66** 2236
[13] Hämäläinen K, Manninen S, Kao C C, Caliebe W, Hastings J B, Bansil A, Kaprzyk S and Platzman P M 1996 *Phys. Rev.* B **54** 5453
[14] Itou M, Sakurai Y, Ohata T, Bansil A, Kaprzyk S, Tanaka Y, Kawata H and Shiotani N 1998 *J. Phys. Chem Solids* **59** 99
[15] Sakai N, Shiotani N, Itoh F, Mao O, Ito M, Kawata H, Amemiya Y and Ando M 1989 *J. Phys. Soc. Japan* **58** 3270
[16] Blaas C 1997 *Thesis* Technische Universitot Wien
[17] Shiotani N, Tanaka Y, Sakurai Y, Sakai N, Ito M, Itoh F, Iwazumi T and Kawata H 1993 *J. Phys. Soc. Japan* **62** 239
[18] Sakurai Y, Tanaka Y, Ohata T, Watanabe Y, Nanao S, Ushigami Y, Iwazumi T, Kawata H and Shiotani N 1994 *J. Phys.: Condens. Matter* **6** 9469
[19] Bellin Ch, Loupias G, Manuel A A, Jarlborg T, Sakurai Y, Tanaka Y and Shiotani N 1995 *Solid State Commun.* **96** 563
[20] Manninen S, Honkimöki V, Hämäläinen K, Laukkanen J, Blaas C, Redinger J, McCarthy J and Suortti P 1996 *Phys. Rev.* B **53** 7714
[21] Pattison P, Hansen N K and Schneider J 1982 *Z. Phys.* B **46** 285
[22] Bauer G E W and Schneider J R 1984 *Phys. Rev. Lett.* **52** 2061
[23] Sakurai Y, Kaprzyk S, Bansil A, Tanaka Y, Stutz G, Kawata H and Shiotani N 1998 *J. Phys. Chem. Solids* submitted
[24] von Barth U and Hedin L 1972 *J. Phys. C: Solid State Phys.* **5** 1629
[25] Biggs F, Mendelsohn L B and Mann J B 1975 *At. Data Nucl. Data Tables* **16** 201
[26] Lam L and Platzman P M 1974 *Phys. Rev.* B **9** 5122
[27] Bauer G E W 1983 *Phys. Rev.* B **27** 5912
[28] Bauer G E W and Schneider J R 1985 *Phys. Rev.* B **31** 681
[29] Hedin L 1965 *Phys. Rev.* A **139** 796
[30] Shoenberg D 1962 *Phil. Trans. R. Soc.* A **255** 85